ETH
Eidgenössische Technische Hochschule Zürich
Swiss Federal Institute of Technology Zurich

Genehmigung des Forschungsplans
(Definitive Zulassung zum Doktorat)

Approval of the Research Plan
(Full admission to doctoral studies)

Studierenden-Nummer
student number 17 - 902 - 594

Name
family name Sinkunaite

Vorname
first name Laura Paulina

Departement
department D - PHYS

Der Forschungsplan wurde eingereicht, eingesehen und angenommen durch:
The research plan has been handed in, seen and approved by:

Name Doktorand/in *Name of doctoral student*	Datum *Date*	Unterschrift *Signature*
Name Dissertationsleiter/in *Name of supervisor*	Datum *Date*	Unterschrift *Signature*
Name Bevollmächtigter Doktoratsausschuss *Name of representative of doctoral board*	Datum *Date*	Unterschrift *Signature*

Für Kandidaten mit Zulassungsprüfung/en:
Die Zulassungsprüfung/en müssen **vor** Genehmigung des Forschungsplans erfüllt sein!

For candidates who have to fulfil further conditions of admission:
*These conditions must be fulfilled **before** the research plan can be approved!*

Frist für Einreichung des Forschungsplans

Frühestens nach erfüllen und offiziell verfügtem Bestehen der Zusatzbedingungen, spätestens ein Jahr nach der Einschreibung

Vorgehen zur Genehmigung des Forschungsplans

Lassen Sie dieses Formular und den Forschungsplan von Ihrer Leiterin / Ihrem Leiter unterzeichnen und senden Sie danach beides an das zuständige **Studiensekretariat**. Dieses kümmert sich um die Unterschrift des Bevollmächtigten des Doktoratsausschusses und schickt das Formular anschliessend an die Doktoratsadministration.

Deadline for submission of the research plan

Only after having passed and received official notification of having successfully fulfilled the further conditions of admission, one year after registration at the latest.

Procedure for approval of your research plan

Please ask your supervisor to sign this form and your research plan and send both to the **Study Administration Office of your department**. They will take care of having it signed by the representative of the doctoral board and will forward it to the Doctoral Administration Office afterwards.

https://www.ethz.ch/studierende/de/doktorat/zulassungspruefung-forschungsplan.html

ETH
Eidgenössische Technische Hochschule Zürich
Swiss Federal Institute of Technology Zurich

Department of Physics

Research Plan

Doctoral thesis:

The detection system for the HyperMu experiment
Doctoral thesis title (provisional)

01.11.2017
Beginning date of doctoral thesis

Doctoral student:

17-902-594
Student number

Laura Paulina Sinkunaite
Name

laura-paulina.sinkunaite@psi.ch
E-mail

Paul Scherrer Institut
Institution (if external doctoral thesis)

Date, signature

Supervisor:

Prof. Dr. Klaus Kirch
Name, title

Date, signature

Co-examiner (if already known):

Name, title

Affiliation

E-mail

Please hand in this form together with the research plan and the form "Approval of the research plan" to the Doctoral Administration Office of D-PHYS

Research Plan

for a Doctoral Study in Physics at the D-PHYS of ETH Zurich

Laura Paulina Šinkūnaitė

1 Introduction and motivation

Proton-radius puzzle The previously conducted measurements [1], [2] of the $2S-2P$ energy splitting in muonic hydrogen (μp) from the triplet ($2S^{F=1}_{1/2} - 2P^{F=2}_{3/2}$) and the singlet ($2S^{F=0}_{1/2} - 2P^{F=1}_{3/2}$) $2S$ sub-levels have shown a 7σ discrepancy comparing to the values extracted from the electron-proton scattering and hydrogen (H) spectroscopy. This so-called "proton-radius puzzle" is interesting for different areas of physics research: verifications of the proton structure at low energies, new determinations of the Rydberg constant, and searches of BSM physics. Moreover, it has triggered various reanalysis of electron-proton scattering data and several new experiments in the field of scattering and atomic physics. So far, the resolution of the "proton-radius puzzle" remains unknown.

Hyperfine splitting The Hyperfine splitting (HFS) is the magnetic moment - magnetic moment interaction. This can be described [3] as

$$\Delta E^{HFS}_{theor} = E^F(1 + \Delta_{QED} + \Delta_{TPE} + \Delta_{weak+HVP}), \tag{1}$$

with E^F denoting the Fermi energy,

$$E^F = \frac{8}{3}\alpha^4 \frac{\mu_p m_1^2 m_2^2}{(m_1 + m_2)^3}, \tag{2}$$

Δ_{TPE}, the two-photon exchange (TPE) contribution (Fig. 1), α, the fine-structure constant, μ_p, the proton magnetic moment, m_1, the muon mass, and m_2, the proton mass. Δ_{QED} represents the QED contribution, $\Delta_{weak+HVP}$ denotes the contribution of hadronic vacuum polarisation (HVP), Δ_{str} is the correction due to the proton structure, and Δ_{pol} is the correction due to the polarisability contribution [4].

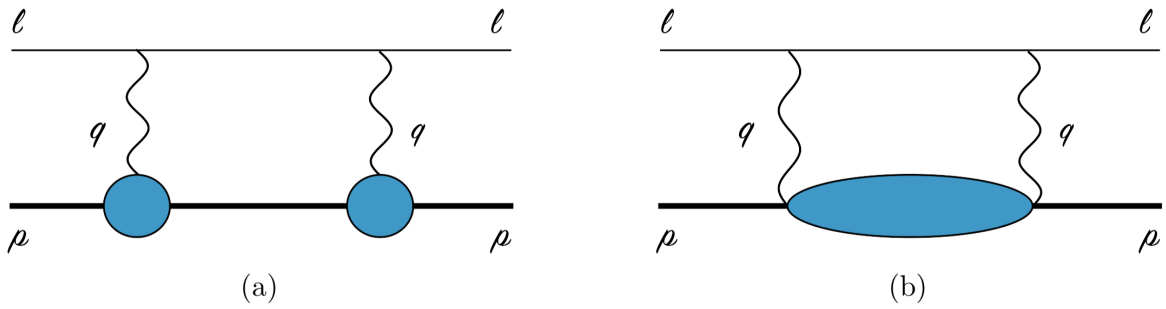

Figure 1: TPE diagrams in forward kinematics: the horizontal lines correspond to the lepton and the nucleus (bold). (a) Elastic contribution to the TPE diagram. (b) Inelastic contribution to the TPE diagram, where the "blob" represents all possible excitations [5].

Two-photon exchange The TPE can be divided into 3 terms,

$$\Delta_{TPE} = \Delta_Z + \Delta_{recoil} + \Delta_{pol}, \tag{3}$$

where the elastic contribution (Zemach) is given by

$$\Delta_Z = \frac{8Z\alpha m_r}{\pi}\int_0^\infty \frac{dQ}{Q^2}\left(G_E(Q^2)\frac{G_M(Q^2)}{1+\kappa_p} - 1\right) = -2(Z\alpha)m_r R_Z, \tag{4}$$

with the Zemach radius defined as

$$R_Z = -\frac{4}{\pi}\int_0^\infty \frac{dQ}{Q^2}\left(G_E(Q^2)\frac{G_M(Q^2)}{1+\kappa_p} - 1\right), \tag{5}$$

where κ_p is a term related to the dipole magnetic moment of the proton. The Zemach radius non-relativistically reduces to the convolution of charge ρ_E and magnetic ρ_M distributions

$$R_Z = \int d^3\boldsymbol{r}|\boldsymbol{r}|\int d^3\boldsymbol{r'}\rho_E(\boldsymbol{r}-\boldsymbol{r'})\rho_M(\boldsymbol{r'}). \tag{6}$$

This is the contribution with the largest uncertainty of the order of 1×10^{-4} of the total HFS. The Δ_{pol} term is the polarisability contribution and the Δ_{recoil} is the negligible recoil correction to the Zemach term. There are two approaches to evaluate the polarisability contribution: using dispersion relations and data such as structure functions and form factors or using chiral perturbation theory. In the dispersive approach, the inelastic contribution can be fully calculated using the measured spin-dependent structure functions of the proton, $g_1(x, Q^2)$ and $g_2(x, Q^2)$ [3].

Motivation The measurement of the $1S - HFS$ transition in the μp with 1 ppm accuracy can be used to evaluate the TPE contribution with a relative accuracy of 1×10^{-4}. This would increase our understanding of the low-energy structure of the proton and would provide a benchmark for chiral perturbation theory, dispersion-based approaches, and lattice QCD. A new experiment (HyperMu) designed to contribute to the resolution of the "proton-radius puzzle" is being developed at the Paul Scherrer Institute (PSI). HyperMu is aiming to measure the ground-state hyperfine splitting ($1S - HFS$) in μp (Fig. 2) with an accuracy of 1 ppm by means of laser spectroscopy. From the successful measurement of the $1S - HFS$ transition, the nuclear-structure - related Δ_{TPE} contribution effects can be determined with a relative accuracy of 1×10^{-4}. In a second step from the TPE, the Zemach radius can be extracted to accuracies of about $\mathcal{O}(10^{-3})$ limited by the theoretical uncertainty of the polarisability contribution. Moreover, the measurement would also be a test of the lepton universality, i.e. when μp laser spectroscopy results are compared to the electron-proton scattering and to the electronic hydrogen (ep) spectroscopy, and on top of that it would impact the resolution of the "proton radius puzzle" and the related "new physics" searches.

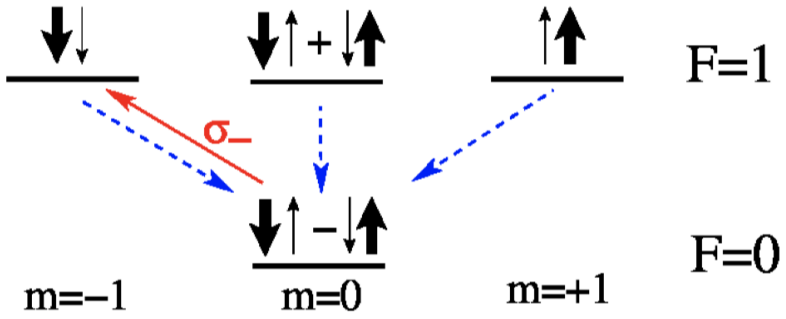

Figure 2: Energy levels and spin compositions of the $1S$ states in μp. The red arrow represents the transition driven by the circularly polarised laser light, the blue arrows illustrate the collisional quenching [3].

2 Working principle

The principle of the HyperMu experiment: Muons are stopped in hydrogen gas forming μp atoms in highly-excited states. The formed μp atoms de-excite to the $F = 0$ sub-level of the ground state (Fig. 2). A high-energy laser pulse (3 mJ at $6.7\mu m$ and 100 MHz bandwidth) excites the μp atoms to the $F = 1$ sub-level of the ground state,

$$\mu p_{F=0} + \gamma \rightarrow \mu p_{F=1}.$$

In collisions with hydrogen molecules (H_2), the μp atoms are de-excited to the $F = 0$ sub-level,

$$\mu p_{F=1} + H_2 \rightarrow \mu p_{F=0} + H_2 + E_{kin}.$$

This transition energy is converted into the kinetic energy. Having this extra kinetic energy, the μp atoms efficiently diffuse to the target walls before muon decays occur. At the target wall, which is made of the high-Z material, the muons are transferred from the μp to the high-Z material forming $(\mu Z)^*$ in an excited state. The highly-excited $(\mu Z)^*$ atoms then de-excite producing MeV X-rays. The MeV X-rays are detected using scintillating detectors (Fig. 3). A resonance curve is obtained by plotting the number of the X-rays versus the laser frequency.

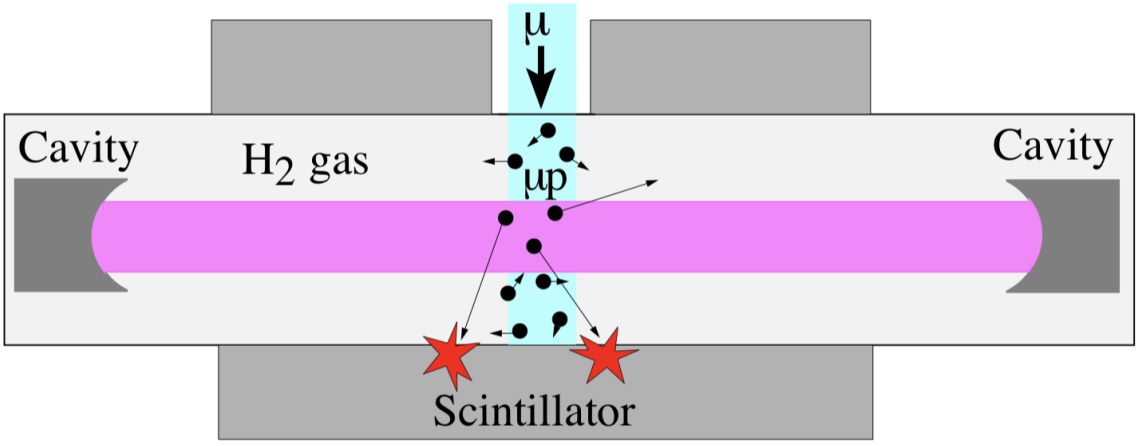

Figure 3: HyperMu experimental scheme showing a laser cavity, muon entrance beam, and the surrounding scintillating detectors [3].

Signal and background The signal events are considered to be the MeV X-rays detected within a time window Δt after the laser excitation. There are two types of background events: intrinsic and erroneous. The intrinsic background is produced by non-laser excited μp atoms, that diffuse to the target walls in the observation time window Δt. This type of background can be minimised by cooling down the target, e.g. keeping the H_2 gas at 50 K temperature. The other type of background arises from the electrons produced in the event of a muon decay, $\mu^- \rightarrow e^- + \overline{\nu_e} + \nu_\mu$, and being falsely identified as X-rays.

Laser system To produce a resonance curve for the $1S - HFS$ transition in the μp, a high-energy laser system delivering 3 mJ pulses with 100 MHz bandwidth at 6.7 μm is needed. We are planning to realise a laser system as depicted in Fig. 4. It is composed of a thin-disk laser followed by optical-parametric down-conversion stages (OPO - OPA) and a difference frequency generating stage (DFG). Using this OPO and OPA scheme, the thin-disk laser needs to be operated in single-frequency mode achieved by injection seeding the thin-disk laser oscillator with an external frequency stabilised continuous-wave (cw) laser at 1030 nm. The pulses

at 1030 nm would then be down-converted in a non-linear crystal to produce two beams, so called an "idler" beam at 2434 nm and a "signal" beam at 1785 nm. The OPO cavity needs to be seeded by a tunable "signal" laser used to scan the resonance. A successive difference frequency generation (DFG) between "idler" and "signal" pulses would then be used to generate 3 mJ pulses at 6.7μm.

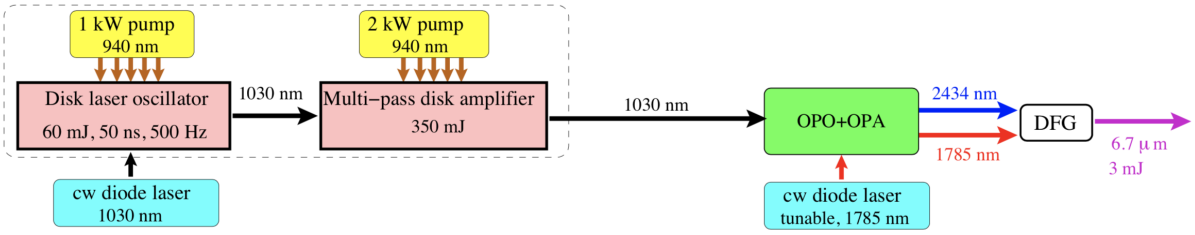

Figure 4: Possible parametric down-conversion laser scheme for μp experiment using OPO and OPA technologies [3].

3 The detection system

Requirements One of the main topics of this thesis is to develop the needed detection system for the HFS experiment. One possible scheme is shown in Fig. 5. The aims of the detection system are listed below.

1. Detection of the incoming muons. The detected signal is used to trigger the Data Acquisition (DAQ) and the laser systems.

2. Measurement of the produced X-ray cascades in the $(\mu Z)^*$ de-excitation process after the μp atoms have diffused to the target wall.

3. Detection of the nuclear capture event. After de-excitation to the ground-state, the muons in the μZ atoms are mainly captured in the nuclear process ($\mu^- + p \rightarrow n + \nu_\mu$).

4. The detection system also needs to measure the electrons from regular muon decays. Those electrons are produced when the μp atoms that do not reach the target wall decay. The nuclear capture rate in the μp atom is much smaller than in high-Z μZ atoms.

5. The detection system must also deal with the background coming from the beam-line and muons stopping in the entrance detector and target window.

For simplicity, in this plan we will only describe the detection of electrons coming from the muon decays and X-rays coming from the muonic X-ray cascade (Table 1).

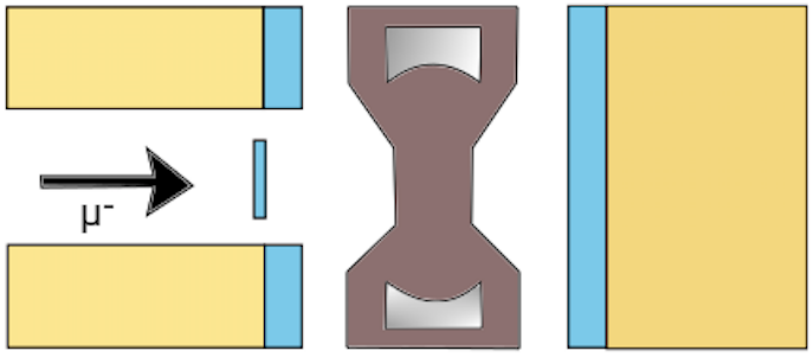

Figure 5: Sketch of the detection system. After the incoming muon beam hits the entrance detector (shown in blue), it enters the target area (brown) with the thoroidal cavity inside (grey). On both down-stream and up-stream parts, series of different thickness plastic scintillators are going to be used (yellow and blue) to detect the X-ray signal and to distinguish it from the background.

Material The ideal material for the detectors would be germanium (Ge) as it provides a good energy resolution. However, its detection rate is too low for HyperMu, therefore we need to use alternative materials that could fulfil the above-listed conditions. We are considering to use thin plastic scintillators to distinguish between a X-ray coming from the cascade event and an electron coming from the muon decay (Fig. 7). Scintillators have a property that the energy

spectrum of cascade events differs considerably from the energy spectrum of an electron from muon decay (Fig. 6). Therefore, a simple energy cut could be used to distinguish between e^- and X-rays.

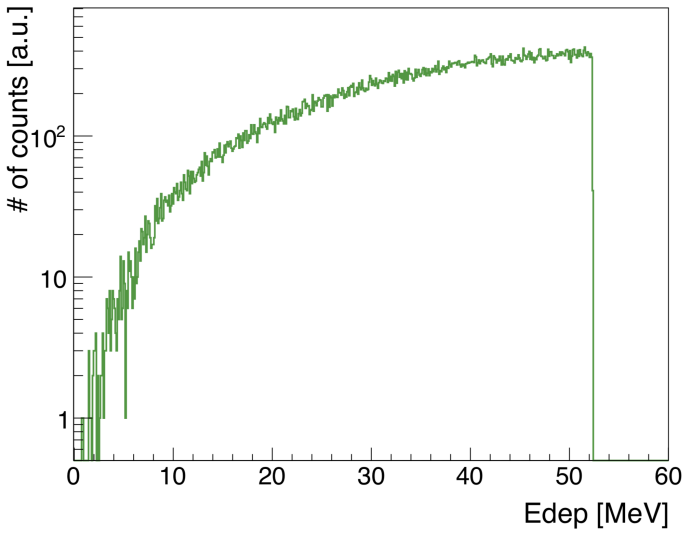

Figure 6: Michel decay spectrum for a muon.

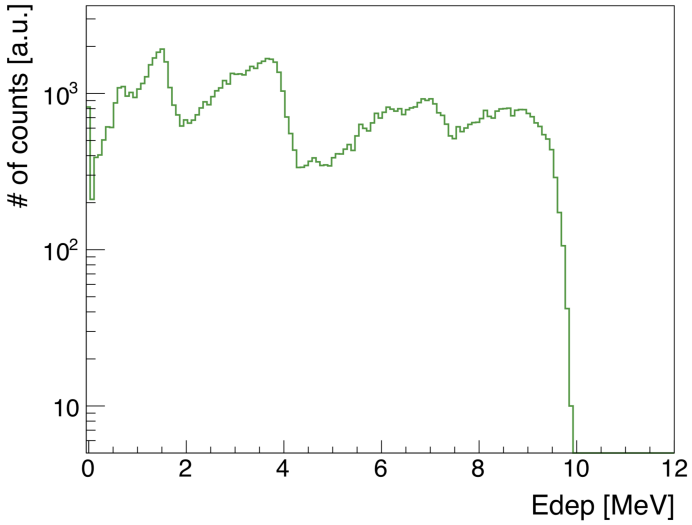

Figure 7: Deposited energy of the X-ray cascade in the thick plastic scintillator.

Table 1: X-ray transitions in gold

Transition $n_i \rightarrow n_j$	Relative probability [$\%$]	Energy [MeV]
$2 \rightarrow 1$	90.00	5.65
$3 \rightarrow 1$	4.50	8.10
$4 \rightarrow 1$	0.30	9.00
$5 \rightarrow 1$	0.10	9.40
$> 6 \rightarrow 1$	1.00	9.60
$3 \rightarrow 2$	84.00	2.40
$4 \rightarrow 2$	6.00	3.30
$5 \rightarrow 2$	1.11	3.70
$6 \rightarrow 2$	0.40	3.90
$> 7 \rightarrow 2$	0.25	4.20
$4 \rightarrow 3$	76.00	0.90
$5 \rightarrow 3$	8.00	1.30
$6 \rightarrow 3$	2.00	1.50
$7 \rightarrow 3$	0.80	1.70
$> 8 \rightarrow 3$	2.50	1.80
$5 \rightarrow 4$	66.00	0.40
$6 \rightarrow 4$	9.00	0.60
$7 \rightarrow 4$	3.00	0.70
$8 \rightarrow 4$	1.00	0.85
$> 9 \rightarrow 4$	4.00	0.90
$6 \rightarrow 5$	64.00	0.22
$7 \rightarrow 5$	11.00	0.36
$8 \rightarrow 5$	3.00	0.45
$9 \rightarrow 5$	1.50	0.52
$> 10 \rightarrow 5$	5.00	0.55
$7 \rightarrow 6$	62.00	0.13
$8 \rightarrow 6$	12.00	0.22
$9 \rightarrow 6$	4.00	0.29
$10 \rightarrow 6$	2.00	0.33
$> 11 \rightarrow 6$	6.00	0.36

Combination of thin and thick scintillators Electrons and X-rays also can be distinguished by considering their total deposited energy. In fact, cascade events have energies up to 10 MeV while the energies of the electrons from the muon decay are distributed according to Fig. 6. Thus, a second energy cut can be applied to the total energy. Therefore, a thicker scintillator that completely absorbs the X-rays and the electrons could be used. Fig. 8 shows an energy spectrum produced with a 50-mm plastic scintillator for the X-ray cascade and the electrons. These two general ideas are the basis of the detection system sketched in Fig. 5. An algorithm distinguishing them can be developed based on the facts that:

- the cascade detection efficiency should be $\geq 50\%$,

- the false identification of electrons as X-rays should be $< 5 \times 10^{-3}$.

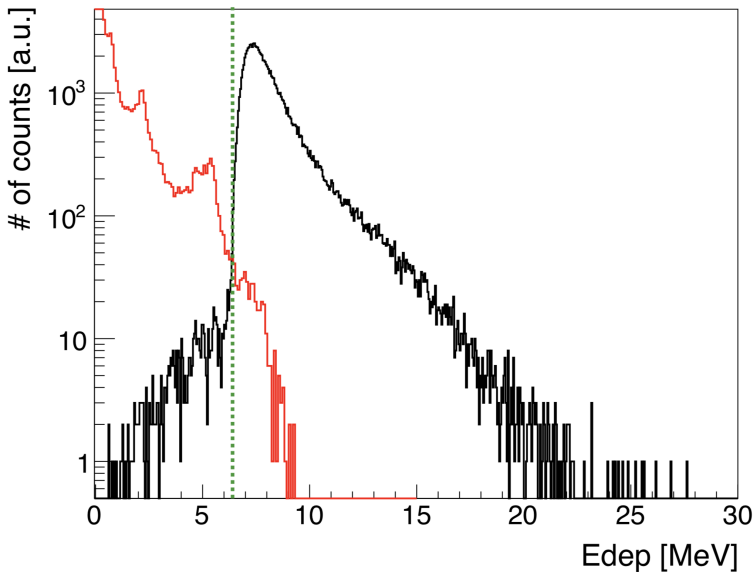

Figure 8: Differences between electrons [black] and X-rays [red] in the energy deposited in the light plastic scintillator. The green dashed line shows a possible location for a cut to separate the particles.

Signal to background ratio The two criteria that can be implemented in the algorithm origin from the signal-to-background ratio. Consider Fig. 9, where A_1 marks the target area and the A_2 marks the laser-excited muon atoms (shown in blue and pink, respectively). Then the background, B, can be expressed as

$$B = d\frac{A_2}{A_1} N_{stopped\,\mu^-} P_{\mu\to e^-\overline{\nu_e}\nu_\mu} \varepsilon_{det} = d\frac{A_2}{A_1} N_{stopped\,\mu^-} \left(1 - e^{-\frac{300ns}{2200ns}}\right), \tag{7}$$

where d is the target width, A_2 is the area of the stopped μ^- atoms, $P_{\mu\to e^-\overline{\nu_e}\nu_\mu}$ is the probability for a muon to decay and produce an electron, and ε_{det} is the detection probability of such an event. The signal, S, on the other hand, can be expressed as

$$S = d'\frac{A_2}{A_1} N_{stopped\,\mu^-} P_{laser-excited} P_{laser-excited\,reach\,the\,wall} \varepsilon_{det}. \tag{8}$$

Here, d' is the width of the laser-excited region, $P_{laser-excited}$ is the probability that the atoms in the region get excited by the laser, $P_{laser-excited\,reach\,the\,wall}$ is the probability that those that had been laser-excited will reach the wall of the target. Now, if we calculate the signal-to-background ratio, some of the parameters cancel out:

$$\frac{S}{B} = \frac{d'}{d}\frac{P_{laser-excited} P_{laser-excited\,reach\,the\,wall}}{\left(1 - e^{-\frac{300ns}{2200ns}}\right)} = \frac{d'}{d}\frac{P_{laser}}{\left(1 - e^{-\frac{300ns}{2200ns}}\right)}, \tag{9}$$

where $\frac{d'}{d}$ is the so-called overlap, P_{laser} is a combined probability that the muonic atom will be laser excited and will reach the wall, and it is equal to $\sim 1\%$. Thus, the ratio S/B is approximately 5×10^{-3}.

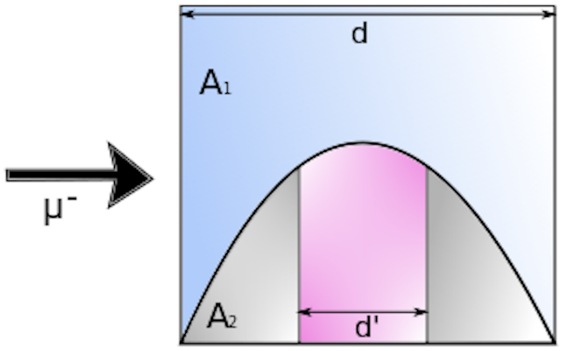

Figure 9: Signal to background ratio.

4 Simulations

Scintillation detectors Traversing the matter, particles lose energy while interacting with the material particles. The interaction mechanisms differ depending whether a particle is neutral or charged. Also, the amount of energy deposited in the material differs depending on the initial energy and the type of the interacting particle. Plastic scintillation detectors can be used to detect these interactions. When excited by ionising radiation, scintillating materials absorb the energy of the incoming particle and re-emit the absorbed energy in the form of light. The generated pulses of light can then be detected by light-sensitive detectors, e.g. photomultiplier tubes (PMT).

Particle interaction with matter When traversing the light plastic scintillating material, electrons continuously lose $\sim 2MeV/cm$. The deposited energy is then converted into the radiation, e.g. photons. This is caused by the bremsstrahlung process, which happens when a highly-energetic charged particle is being deflected in the electric field of an atomic nucleus. On the other hand, when the X-rays travel through the medium, they scatter off the charged particles producing the secondary X-rays and the electrons (the so-called Compton scattering). Those

secondary X-rays can scatter off again generating cascades of the secondary particles. By varying the thickness of the scintillation detectors and the solid angle of their position, one can get a clue about the primary particle.

HypereX The purpose of the detection system (HypereX) for the HyperMu experiment is to detect the MeV X-ray signal events and to reject the erroneous background events caused by the electrons coming from the muon decay (Sec. 2). A system of scintillation detectors can be used to tackle this problem. Different detector geometries and materials are being considered using a Monte Carlo simulation package $G4beamline$ [7] to find an optimal design before its realisation. To judge, whether a geometry is suitable, we introduce the ratio $P_{e\to X}/P_{e\to e}$, where $P_{e\to X}$ is the probability that an electron is misidentified as a X-ray and $P_{X\to X}$ is the X-ray detection efficiency. To accept the geometry as satisfactory, the aforementioned ratio should be larger than the marginal value of 5×10^{-3} that comes from the signal to background ratio (SBR). Two detection schemes that look promising emerge using (1) a magnetic setup or (2) a planar geometry.

Cylindrical detector in a magnetic field One of the detection schemes is employing the usage of a homogeneous 5 T magnetic field surrounding the target and the detection regions (Fig. 10). This would make charged particles spiral along the beam axis and would not allow them to deposit any energy in the hollow cylindrical detector surrounding the beam axis. Thus, the false-identification of the negatively charged electrons would be eliminated. Even though this scheme could provide us with a better beam intensity (due to a better beam focus) and a misidentification probability $P_{e\to X}$ at the required level of $\mathcal{O}(10^{-3})$, simulations have shown (Fig. 11a) that the X-ray detection efficiency $P_{X\to X}$ is well too low the needed $\sim 65\%$ to make up an acceptable ratio $P_{e\to X}/P_{e\to e}$. Other additional disadvantages would be the lack of space for the optical cavity, harder access to the detectors and the experimental mechanics, and finally,

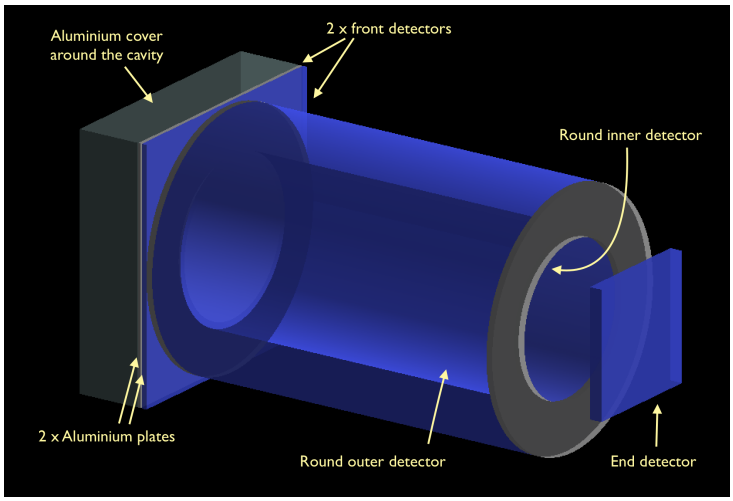

Figure 10: Magnetic setup: a hollow cylindrical scintillation detector in a constant 5 T magnetic field. Aluminium cover imitates a target area, where μp atoms are produced. The inner light plastic scintillation detector is topped up with an outer heavier-Z plastic scintillator or, instead, with a layer of aluminium. Between the target and the cylindrical detector there two thin scintillators surrounded by two aluminium plates. At the end of the cylinder [*on the right*] is yet another light plastic scintillator to detect the spiralling electrons exiting the setup.

increased costs and duration for the magnet's production.

```
for (int i=0; i<iterations;i++)
{
do something
}
```

```
                for (int a=0; a<allvEvIDBD1muNaI[0].size(); a++) {

                   if ((allvEdepSD1muNaI[i][a] < Ethr1) && (allvEdepSD2muNaI[i][a] < Ethr
                      if ((allvEdepBD1muNaI[i][a] > Ethr) && (allvEdepBD1muNaI[i][a] < E
//                          if (((allvEdepSDT1muNaI[i][a] < Ethr3) || (allvEdepSDB1muNa
                            if (((allvEdepSDT1muNaI[i][a] < Ethr3) && (allvEdepSDB1muNa
                                  eXrayN2NaI += 1;
                               } else { eelecN2NaI += 1; }
                         } else { eelecN2NaI += 1; }
                   } else { eelecN2NaI += 1; }
```

```
if (E1 < 0.5) {
   if (E2}
```

Detector with a planar geometry Another feasible detection scheme would consist of layers of parallelepiped-shaped scintillation detectors of varying thickness (Figs. 11a and 11b). Initial

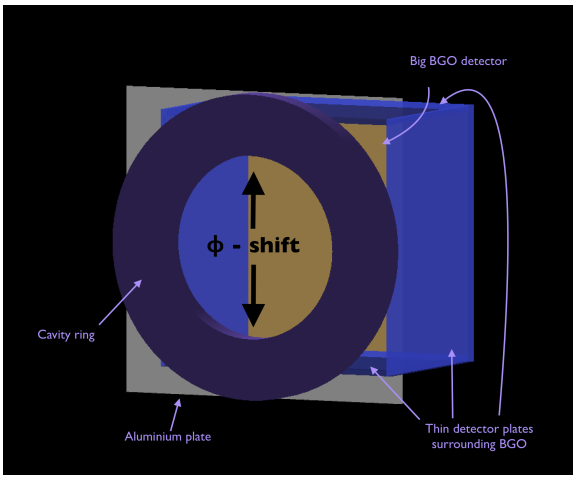

(a) Φ-shift: changing the inner and outer diameters of the cavity mechanics (shown as a purple ring). A thin aluminium plate is placed behind the cavity representing a target wall. It is followed by a big BGO detector that is surrounded with plates of light plastic scintillation detectors from both sides, top, and the bottom.

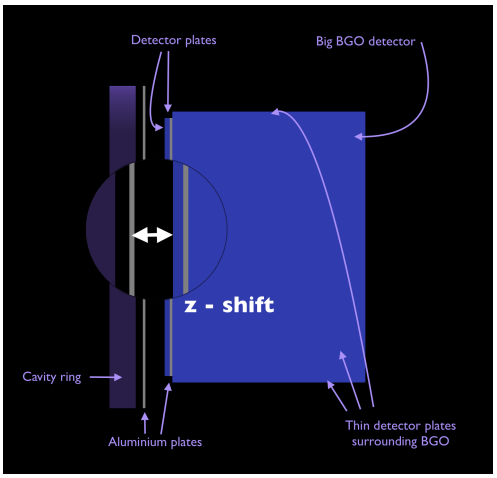

(b) z-shift: moving the detectors away from the target. A lateral view to the planar-geometry detection scheme shows two aluminium plates with two thin light plastic scintillation detectors in between them. The big BGO scintillation detector and it surrounding light plastic scintillation detectors are shown on the right.

Figure 11: Planar detector geometry: various layers of scintillating parallelepipeds of varying thickness.

simulations have shown that a change in the transverse and/or lateral size of the scintillators reveals a different behaviour in the energy deposition for the signal and background particles. It was noticed, that the thicker the detector is, the more likely that a X-ray will deposit some energy in it. The wider it is, thus the bigger solid angle is covered, and the more hits of the particles that scatter off it detects. Moving the detectors away from the optical cavity, i.e. introducing a z-shift, and changing the diameter of the mechanics surrounding the target, i.e. introducing a ϕ-shift, also shows some significant differences (Figures 12b).

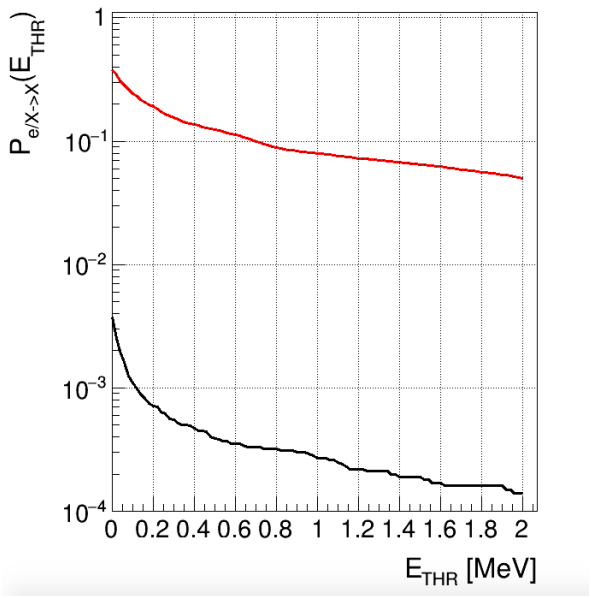

(a) The e^- misidentification probability $P_{e\to X}$ [*black*] and the X-ray detection efficiency $P_{X\to X}$ [*red*] as obtained for the scenario with a magnetic setup.

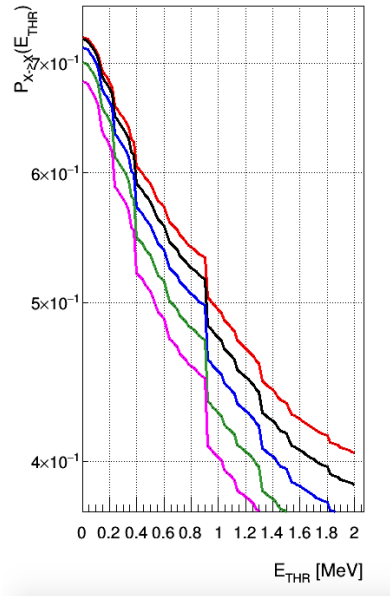

(b) The variance in the $P_{X\to X}$ for a planar setup. Different curves are obtained introducing a constant 50-mm ϕ-shift and 0-mm, 25-mm, 50-mm, 75-mm, and 100-mm z-shift.

Figure 12: X-ray detection efficiency and electron misidentification as a X-ray probability plotted versus a lower energy threshold E_{THR} applied to the scintillation detectors. This can be thought of as a benchmark to cut some of the background events in the low-energy region, $< E_{THR}$.

Further steps The next step is to introduce the missing physical processes into the simulation package, i.e. nuclear capture and muon transfer to gold. After re-optimisation of the already considered parameters and after reaching a high enough X-ray detection efficiency $P_{X\to X}$ and a low enough $P_{e\to X}$ probability in the simulations, a design will be established for the manufacture. One of the beam times will be used to test this design.

5 Schedule of the research work

1st year [2017 - 2018] (done)

- Initial detection simulations
- Observation of the development of the single-frequency external cavity tapered amplifier laser system by the researchers from the National Tsing Hua University in Taiwan.
- Further detection simulations:
  - Geometry, detector materials.
  - Event - by - event analysis.

2nd year [2018 - 2019]

- Advanced detection simulations:
  - Implementation of the advanced physical processes: nuclear capture and muon transfer.
- Writing of a technical summary of the detector simulations.
- Study the μ^- beam when focused with a small solenoid (if time permits).
- Simulation of an alternative beam-line in $\pi e5$ (if time permits).

- Measurements:
  - Test of the detection system.
  - Test of the diffusion processes at various temperatures to validate Jonas Nuber's simulations.
  - Measure stopping efficiencies.
- Initial work on Optical Parametric Oscillator (OPO), Optical Parametric Amplifier (OPA), and Difference-Frequency Generator (DFG):
  - Check the various schemes and various crystal materials.
  - Simulation of the scheme and its optimisation.
  - Test of the scheme in the laboratory.

3rd year [2019 - 2020]

- Further work on OPO, OPA, and DFG:
  - Characterisation of the pulse output.
  - Spectroscopy of the absorption lines.
- Contribution to the total setup:
  - Development and installation of the data acquisition (DAQ) system.
  - Target finalisation and installation.
  - Detector finalisation and installation.
  - Laser system's finalisation and installation.
- Beam-time, Physics run.
- Analysis of the beam-time data.
- Writing of the thesis.

6 Teaching activities

Previous teaching duties were:

- 2018 - Teaching assistant for General Physics 2 (FS, Prof. K. Kirch)
- 2018 - Proton Irradiation Facility (PIF) shift operator (HS, Dr. W. Hajdas)

Further activities are planned at the PIF at PSI and should occupy $10 - 13\%$ of the total workload, as needed.

References

[1] The CREMA collaboration. *Laser Spectroscopy of Muonic Atoms and Ions*. arXiv: 1609.03440v1, 2016.

[2] Aldo Antognini, Franz Kottmann, François Biraben, Paul Indelicato, François Nez, and Randolf Pohl. *Theory of the $2S - 2P$ Lamb shift and $2S$ hyperfine splitting in muonic hydrogen*. arXiv: 1208.2637v2, 2012.

[3] The CREMA collaboration. *Proposal for an experiment at PSI: Hyperfine splittings in muonic hydrogen and 3He*. 2016.

[4] R. N. Faustov and A. P. Martynenko. *Muonic hydrogen ground state hyperine splitting*. arXiv: hep-ph/0312116v2, 2004.

[5] Franziska Hagelstein. *PhD thesis: Exciting nucleons in Compton scattering and hydrogen-like atoms*. arXiv: 1710.00874v1, 2017.

[6] Xiaobing Xie et al. *Injection-seeded single frequency* $2.05\ \mu m$ *output by ring cavity optical parametric oscillator*. Chinese Optics Letters, **15**(9), 2017.

[7] G4beamline software, `http://www.muonsinternal.com/muons3/G4beamline`.